

Discovery of fully synthetic FKBP12-mTOR molecular glues

Robin C. E. Deutscher⁺,^[1] Christian Meyners⁺,^[1] Maximilian L. Repity,^[1] Wisely Oki Sugiarto,^[1] Jürgen M. Kolos,^[1] Edvaldo Maciel,^[1] Tim Heymann,^[1] Thomas M. Geiger,^[1] Stefan Knapp,^[2] Frederik Lermyte,^[1] and Felix Hausch^{*[1,3]}

[1] Institute for Organic Chemistry and Biochemistry, Technical University Darmstadt, Peter-Grünberg-Straße 4, 64287 Darmstadt (Germany).

[2] Institut für Pharmazeutische Chemie, Goethe-University Frankfurt, Biozentrum, Max-von-Laue-Str. 9, 60438 Frankfurt am Main, Germany and Structural Genomics Consortium, Goethe-University Frankfurt, Buchmann Institute for Life Sciences, Max-von-Laue-Str. 15, 60438 Frankfurt am Main; German Cancer Consortium (DKTK)/German Cancer Research Center (DKFZ), DKTK site Frankfurt-Mainz, 69120 Heidelberg, Germany

[3] Centre for Synthetic Biology, Technical University of Darmstadt, 64287 Darmstadt (Germany)

*Correspondence: felix.hausch@tu-darmstadt.de

[*] These authors contributed equally

Abstract: Molecular glues are a class of drug modalities with the potential to engage otherwise undruggable targets. However, the rational discovery of molecular glues for desired targets is a major challenge and most known molecular glues have been discovered by serendipity. Here we present the first fully synthetic FKBP12-mTOR molecular glues, which were discovered from a FKBP-focused, target-unbiased ligand library. Our biochemical screening of >1000 in-house FKBP ligands yielded one hit that induced dimerization of FKBP12 and the FRB domain of mTOR. The crystal structure of the ternary complex revealed that the hit targeted a similar surface on FRB domain compared to natural product rapamycin but with a radically different interaction pattern. Structure-guided optimization improved potency 500-fold and led to compounds, which initiate FKBP12-FRB complex formation in cells. Our results show that molecular glues targeting flat surfaces can be discovered by focused screening and support the use of FKBP12 as a versatile presenter protein for molecular glues.

Introduction: For a long time, intracellular proteins without suitable ligand binding pockets have been considered undruggable. The discovery of molecular glues as a drug modality challenged that notion¹. Through the help of an additional protein - a presenter protein - the available binding surface of the molecular glue-protein-complex can become large enough to bind even flat, featureless target protein surfaces with high affinity²⁻⁴. If the presenter protein is an E3 ligase, the degradation of the target protein through the proteasome machinery can be enabled, providing molecular glue degraders^{5,6}. Unfortunately, both molecular glues and molecular glue degraders are still largely discovered by serendipity as approaches to identify them by a more rational strategy are rare⁷. The first and most prominent examples for the serendipitous discovery of molecular glues are the clinically used immunosuppressants rapamycin **1**, FK506 **2** and cyclosporin A **3** (Fig. 1)⁸⁻¹⁰.

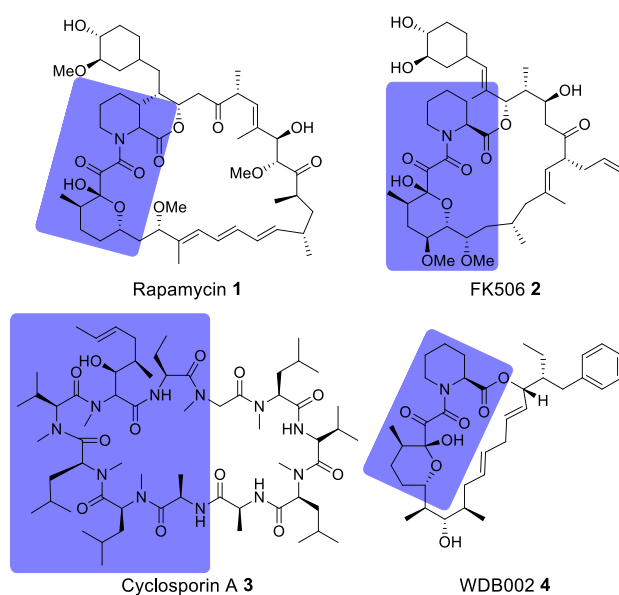


Figure 1. Natural product molecular glues rapamycin **1**, FK506 **2**, cyclosporine A **3** and WDB002 **4**. FKBP12 or Cyp18 binding moieties are highlighted in slate blue.

Being among the first of their kind, their cellular function was discovered first, followed by the identification of the presenter protein, and finally the target protein itself. FK506 **2** and cyclosporin A **3** are now known to bind to FKBP12 (FK506 binding protein 12) and cyclophilin 18 (Cyp18), respectively, and their binary complexes bind to calcineurin, blocking access to its substrate binding site^{11–13}. Rapamycin **1** binds to FKBP12 and then their complex binds to the FRB (FKBP-rapamycin **1** binding) domain of mTOR (mechanistic target of rapamycin **1**), thereby inhibiting functions of the mTORC1 complex¹⁴.

FKBP12 and Cyp18 might be preferred presenter proteins as nature used them repeatedly for molecular glues, with additional examples being WDB002 **4** (Fig. 1), inducing FKBP12-CEP250 complexes¹⁵, and sanglifehrin A, which was shown to induce Cyp18-IMP2 complexes^{16,17}. For the natural product Antascomycin B,¹⁸ we recently showed that it stabilizes the interaction between the larger FKBP51 and the kinase AKT.¹⁹ Furthermore, there are several other FKBP12-binding natural products (e.g. Meridamycin)²⁰ that can be considered orphan molecular glues, as their postulated ternary target proteins have not yet been identified.²¹ Recently, rapamycin **1** analog libraries (rapafucins) have been developed by Liu and coworkers²² as potential synthetic FKBP-based molecular glues, which led to inhibitors for hENT1,²² GLUT1,²³ and PAANIB-1.²⁴ Based on early work by WarpDriveBio, the company Revolution Medicines developed the Cyp18-based covalent-reactive KRAS^{G12C} inhibitors RMC-4998 and RMC-6291,²⁵ with the latter currently being investigated in a phase I clinical trial (NCT05462717).²⁶ Based on the scaffold of RMC-6291, the pan-RAS inhibitors RMC-7977 and RMC-6236 were developed^{27,28}, the latter of which is also investigated in a phase I clinical trial (NCT05379985).²⁹ As of today there is no universally applicable strategy to systematically identify molecular glue hits³⁰ and little is known about the prospects for subsequent optimization.

Results and Discussion: To explore the likelihood to discover novel molecular glues from scratch, we used FKBP12 and the FRB domain of mTOR as a well-established model system. We opted for a HTRF (homogeneous time-resolved fluorescence) screening assay using a His-eGFP-FKBP12 and GST-tagged FRB constructs. To enable the detection of weak initial hits, we optimized the assay conditions to allow for high compound concentrations (Fig. S1). Using this assay, we screened our internal compound library containing >1000 FKBP focused ligands (Fig. 2A), originally developed for human FKBP51 or bacterial FKBP5s (Fig. S2).^{31–44}

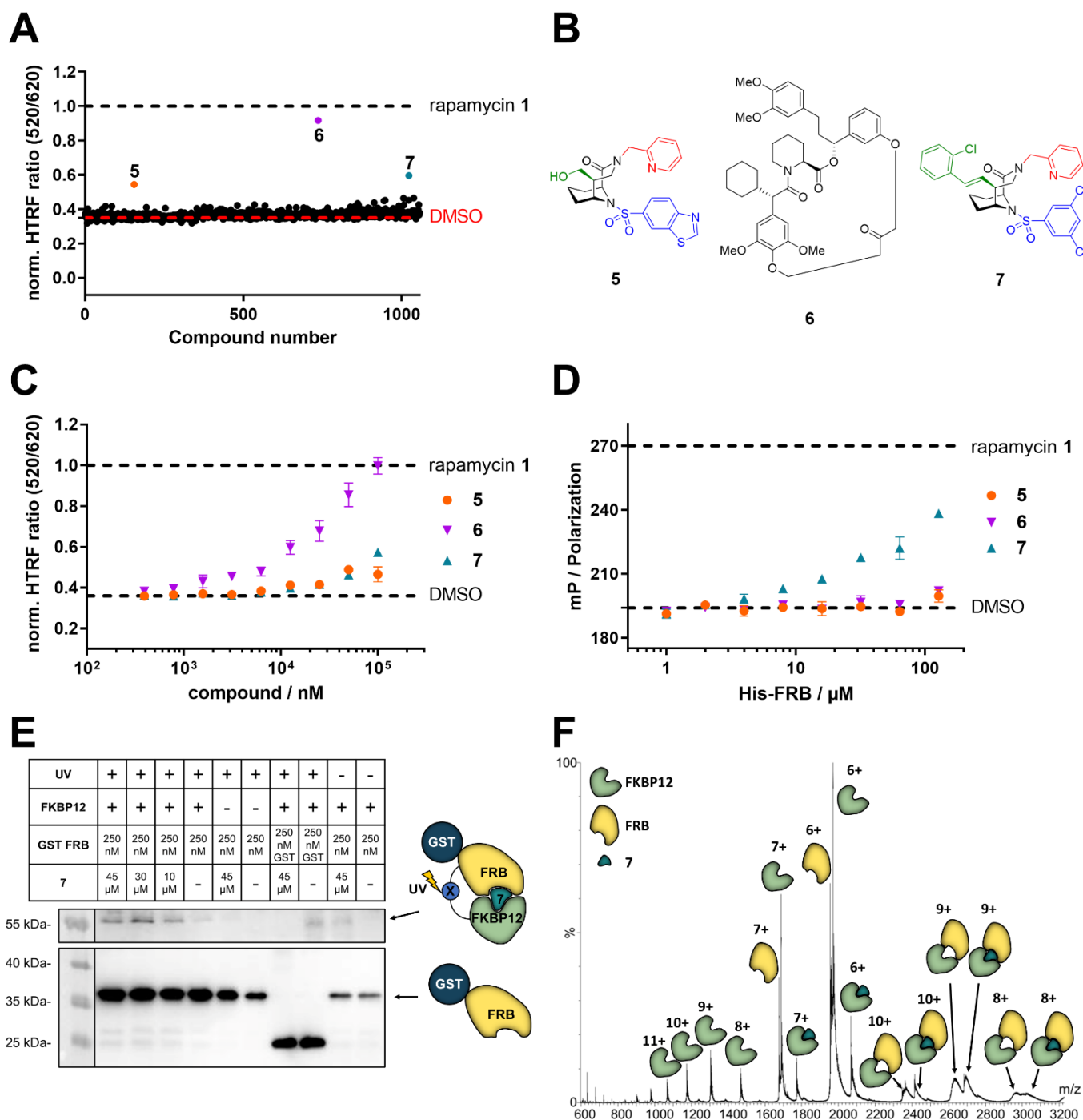


Figure 2. Identification of compound 7 as a FKBP12-FRB molecular glue. **A** Initial HTRF screening for the compound-induced formation of the ternary FKBP12-FRB complex using 100 μM His-eGFP-FKBP12, 20 nM GST-FRB and 1 nM terbium-labelled anti-GST antibody, data are represented as mean. **B** Structure of the three initial screening hits 5^{31} , 6^{40} and 7^{45} . **C** Compounds 5, 6, and 7 dose-dependently increase the HTRF signal indicative of induced proximity between His-eGFP-FKBP12 and the terbium-labelled antibody/GST-FRB complex, data are represented as mean \pm SEM. **D** Compound 7, but not 5 or 6, increases polarization in a FRB dose-dependent fluorescence polarization assay using 20 nM fluorescein-labelled FKBP12^{E140C} and 5 μM compound, data are represented as mean \pm SEM. **E** Western-Blot of photoreactive, diazirine labelled FKBP12^{T43C} mutants photo-crosslinked with GST-FRB. UV light-induced GST-reactive bands at a size of approx. 55 kDa are indicative of the ternary complex of compound 7, FKBP12 and FRB being formed in vitro. **F** Native mass spectrum of the FKBP12-7-FRB complex acquired under soft conditions to maintain the non-covalent interactions. The ternary complex is present in three charge states (8+, 9+, and 10+). The presence of additional peaks of intermediary species (e.g., protein subunits, etc) is typical as no isolation of a specific peak was performed. (**A**, **C**, **D**) Rapamycin 1 and DMSO were used as positive and negative controls, respectively.

Three hits, compounds **5**,³¹ **6**⁴⁰ and **7**⁴⁵ (Fig. 2B), were identified to induce a HTRF signal in a dose-dependent manner (Fig. 2C). However, only compound **7** dose-dependently induced higher fluorescence polarization, indicative of ternary complex formation, in an orthogonal fluorescence polarization (FP) assay with fluorescein-labelled FKBP12 in the presence of high concentrations of FRB (Fig. 2D). For compound **6**, we were able to attribute the strong activity in the HTRF-assay to compound-induced binding of His-eGFP-FKBP12 directly to the anti-GST antibody (Fig. S3). The desired activity of compound **7** was further validated by in vitro photo crosslinking experiments using FKBP12 site-specifically labelled with a photo crosslinking moiety (Fig. 2E) and native MS experiments (Fig. 2F and Fig. S5). With these three experiments we firmly validated the weak molecular glue activity of compound **7**.

To clarify the molecular binding mode, we determined the cocrystal structure of the FKBP12-**7**-FRB ternary complex (Fig. 3A). The binding of compound **7** to FKBP12 was similar as observed with related ligands from the [4.3.1]-bicyclic sulfonamide class⁴⁶ and all key interactions were conserved (e.g. hydrogen bonds to the backbone NH of Ile⁵⁶ or to the phenol of Tyr⁸², Fig. 3B).

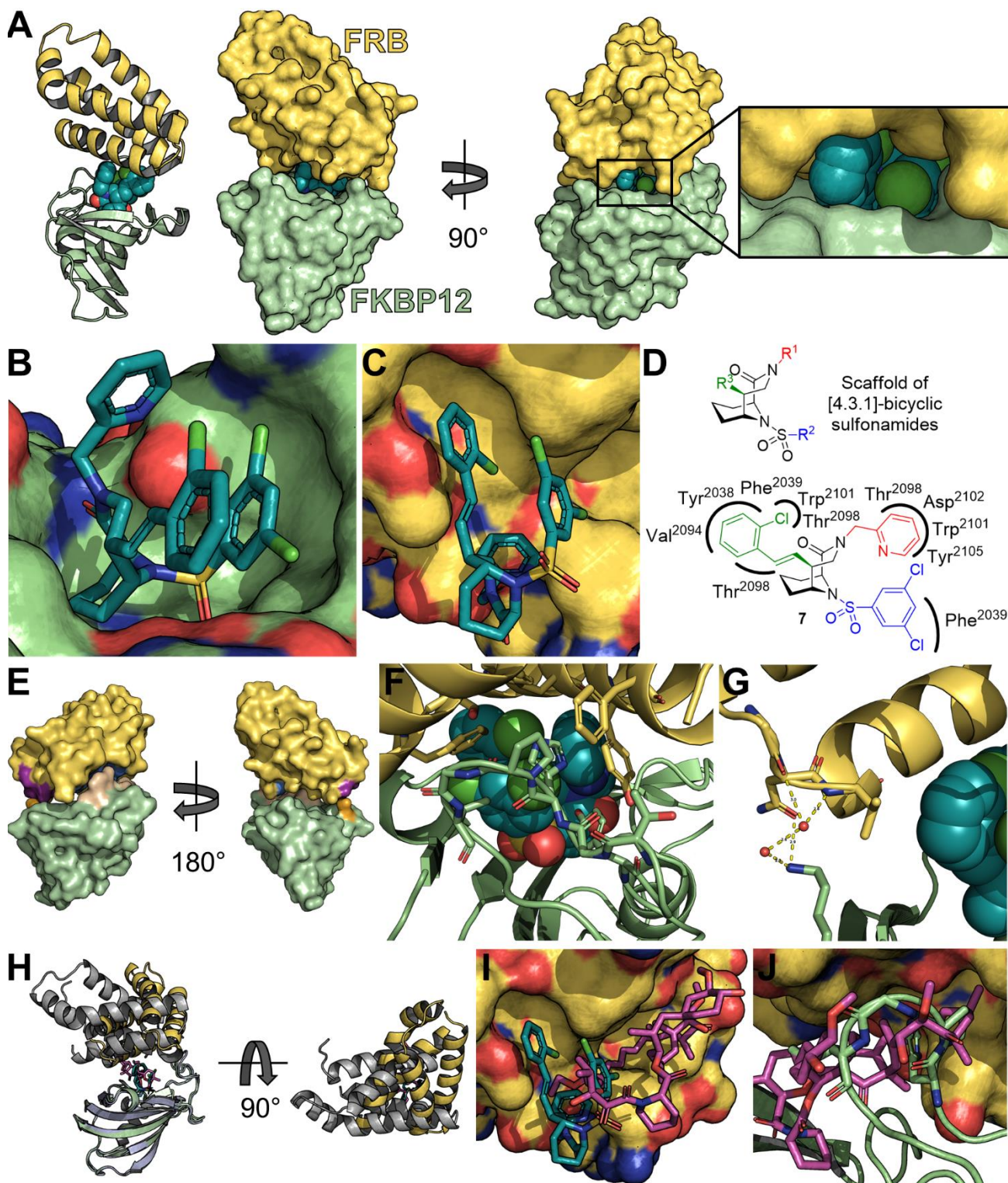


Figure 3. Cocystal structure of the FKBP12-7-FRB ternary complex (PDB: 8PPZ). **A** Structure of overall complex of compound **7** (spheres in dark cyan), FKBP12 (surface or cartoon in light green) and FRB (surface or cartoon in yellow). **B** Binding mode of compound **7** (dark cyan sticks) towards FKBP12 (light green surface) in the ternary complex. FRB omitted for clarity. **C** Binding mode of compound **7** (dark cyan sticks) towards FRB (yellow surface) in the ternary complex. FKBP12 omitted for clarity. **D** Scaffold of [4.3.1]-bicyclic sulfonamides with R¹-position substituents in red, R²-position substituents in blue and R³-position substituents in green and two-dimensional interaction map of compound **7** with the FRB domain of mTOR. **E** FKBP12 (shown as green surface) and FRB (shown as yellow surface) with direct amino acid contacts coloured in wheat and orange for FKBP12 and marine and purple for FRB (primary and secondary interaction sites, respectively). **F** Complex of FKBP12, FRB and compound **7** (dark cyan spheres) with amino acids participating in primary and secondary direct contacts shown as sticks. **G** Complex of FKBP12, FRB and compound **7** (dark cyan spheres) with amino acids participating in secondary direct contacts between FKBP12 and FRB shown as sticks. Water and water-mediated hydrogen bond are shown as red spheres and yellow dashes. **H** Overlay of FKBP12 derived from the ternary

complexes with compound **7**, FKBP12 and FRB (PDB: 8PPZ) with the ternary complex of rapamycin **1**, FKBP12 and FRB (PDB: 1NSG). FKBP12 molecules were partially omitted for clarity. Rapamycin **1** (magenta sticks) and compound **7** (dark cyan sticks) lead to different orientations of FRB (yellow for complex with compound **7**, grey in complex with rapamycin **1**). **I** Overlay of FRB of the cocrystal structures of compound **7** (dark cyan sticks, FKBP12 omitted for clarity) with the cocrystal structure of rapamycin **1** (magenta sticks, FRB in gray), highlighting the different binding mode of both complexes. **J** Overlay of FRB derived from the cocrystal structure with compound **7** (FKBP12 shown in green cartoon and sticks, FRB as yellow surface, **7** not shown) with the cocrystal structure of rapamycin **1** (magenta sticks, PDB: 1NSG).

The interactions between compound **7** and FRB were largely hydrophobic in nature (Fig. 3C&D). All three substituents (R^1 , R^2 and R^3) of the [4.3.1]-bicyclic core engaged in contacts with the FRB domain (Fig. 3C). The R^1 -pyridine formed van-der-Waals contacts with Thr²⁰⁹⁸, Trp²¹⁰¹, Asp²¹⁰² and Tyr²¹⁰⁵. One chlorine and the para-position of the R^2 -phenyl ring formed van-der-Waals contacts with Phe²⁰³⁹. The R^3 -substituent of compound **7** formed most interactions with the FRB domain, incl. van-der-Waals contacts to Tyr²⁰³⁸, Phe²⁰³⁹, Val²⁰⁹⁴, Thr²⁰⁹⁸ and Trp²¹⁰¹.

Several direct contacts between FKBP12 and FRB were observed, located in two regions (Fig. 3E). The major contacts were formed between the 80s loop of FKBP12 (Tyr⁸² and Thr⁸⁵-Ile⁹⁰) and the side chains of Ser²⁰³⁵, Phe²⁰³⁹, Trp²¹⁰¹, Tyr²¹⁰⁵, and Phe²¹⁰⁸ of FRB (Fig. 3F). This included a direct hydrogen bond from the phenol group of Tyr²¹⁰⁵ (FRB) to the backbone carbonyl of Gly⁸⁶ (FKBP12). In the second region, the amine group of Lys⁴⁴ of FKBP12 formed a hydrogen bond to the primary amide carbonyl bond of Asn²⁰⁹³ (FRB), as well as a hydrogen bond to Gly²⁰⁹², which was mediated by two water molecules (Fig. 3G). The side chain of Lys⁴⁴ of FKBP12 also formed van-der-Waals contacts with Val²⁰⁹⁴ of the FRB domain.

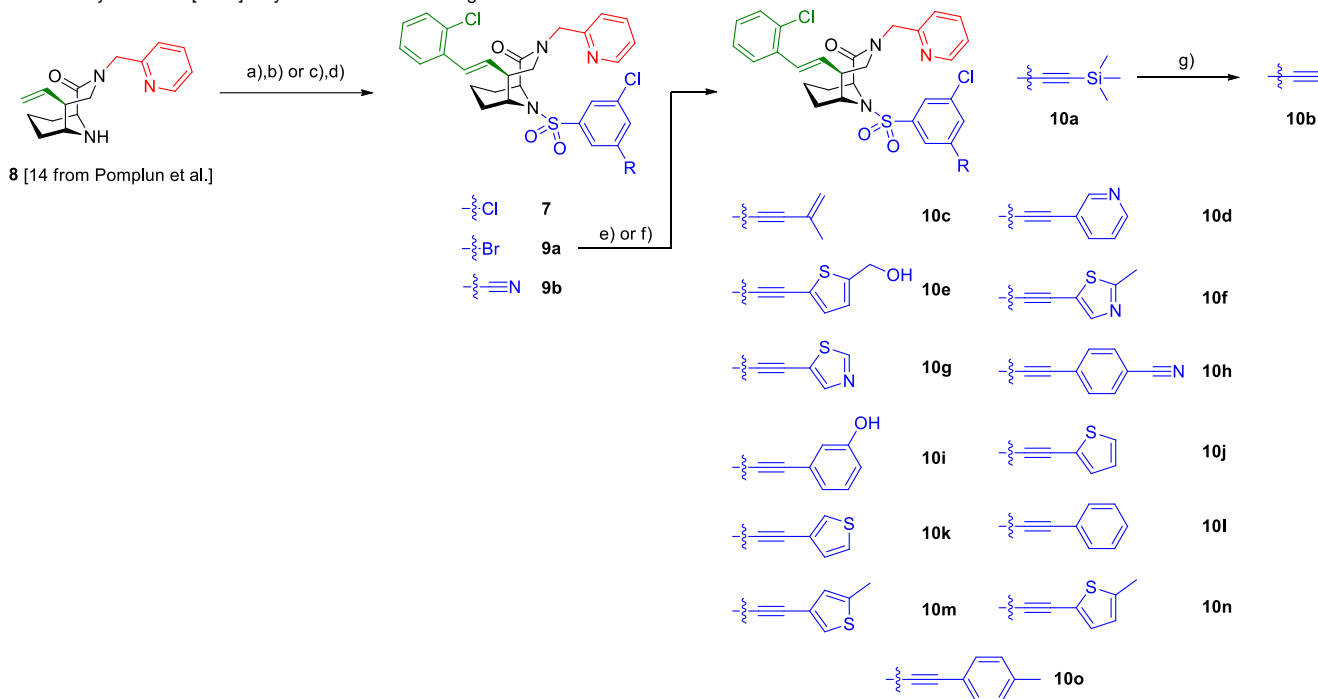
The comparison with the known FKBP12-rapamycin **1**-FRB ternary complex (PDB: 1NSG)⁴⁷ revealed that the FKBP12-**7** and FKBP12-rapamycin **1** binary complexes target a similar surface region on FRB. However, the specific interactions radically differed since the orientation of the FRB was rotated by 90° between the two ternary complexes. (Fig. 3H). While the binding surface on the FRB domain partially matched for compound **7** and rapamycin **1**, both also formed unique interactions with parts of the FRB-domain (Fig. 3I). Interestingly, in the FKBP12-**7**-FRB complex the 80s loop of FKBP12 mimicked some of the interactions formed by the conjugated triene moiety of rapamycin **1** in the FKBP12-**1**-FRB complex (Fig. 3J).

The total binding interface, calculated with PISA⁴⁸, between the FKBP12-**7** complex and the FRB-domain was 632 Å², which was similar to the interaction surface between the FKBP12-rapamycin **1** complex and FRB (698 Å²). However, the contributions of the compounds vs. FKBP12 differed substantially. While in the FKBP12-**7**-FRB complex, 194 Å² of the contact surface were contributed by compound **7** and 428 Å² by 'direct' contacts of FKBP12, in the FKBP12-rapamycin **1**-FRB complex 395 Å² were contributed by rapamycin **1** and 303 Å² by FKBP12.

To increase the weak potency of the initial hit **7** utilizing the structure of the ternary complex, we studied the role of the chlorine pointing into a small cavity between FKBP12 and the FRB domain (Fig. 3A insert, chlorine shown as green sphere). To explore this position, we substituted one of the meta chlorines with small substituents such as bromine, nitrile, and acetylene (Scheme 1). This led to compounds **9a/b** and **10a/b** with slightly improved potencies for ternary complex induction (Tab. 1). Gratifyingly, the extension of the acetylene by an additional substituent like allyl, phenyl rings and heterocycles substantially enhanced the ternary complex formation 12- to 500-fold. Although addition of an allyl group (**10c**) already brought potency down below 10 μM, a full phenyl ring (**10l**) enhanced the potency 175-fold. Hydrophobic substituents on the phenyl ring, for example methyl (**10o**), were better tolerated, while more hydrophilic substituents, e.g. hydroxy (**10i**) and nitrile (**10h**) reduced ternary complex formation. Thiophenes (**10j**, **10k**), thiazoles (**10f**,

10g) and methylthiophenes (**10e**, **10m**, **10n**) all induced formation of the ternary complex with $<2 \mu\text{M}$ potency in the FP-assay. Similarly to the phenyl rings, more hydrophilic substituents perform worse regarding the ternary complex potency. All analogs retained high affinity to purified FKBP12 alone ($K_i < 12 \text{ nM}$) and occupied FKBP12 inside human cells with an IC_{50} between 40-7500 nM (Tab. 1).

Scheme 1. Synthesis of [4.3.1]-bicyclic sulfonamide analogs.


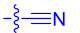
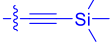

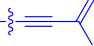
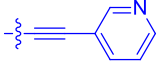
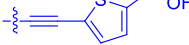
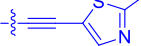


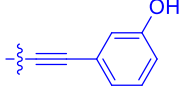

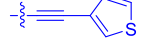
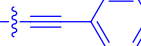
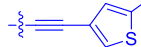
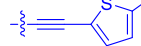



Reactions and conditions: a) sulfonyl chloride, DIPEA, MeCN, rt, compound **7**: 18, 48 % yield, **9b**: 16 h, 49 % yield; b) 1-bromo-2-chlorobenzene, K_2CO_3 , $\text{Pd}(\text{dppf})\text{Cl}_2 \cdot \text{CH}_2\text{Cl}_2$, 100°C , compound **7**: dioxane, 40 h, 57 % yield, **9b**: DMF, 18 h, 25 % yield; c) 1-bromo-2-chlorobenzene, K_2CO_3 , $\text{Pd}(\text{dppf})\text{Cl}_2 \cdot \text{CH}_2\text{Cl}_2$, dioxane:H₂O=20:1, 100°C , 19 h, 78 % yield; d) 3-bromo-5-chlorosulfonyl chloride, DIPEA, MeCN, rt, 46 h, 55 % yield; e) alkyne, $\text{Pd}(\text{PPh}_3)_4$ or $\text{Pd}(\text{dppf})\text{Cl}_2 \cdot \text{CH}_2\text{Cl}_2$, CuI, TMEDA, $80-90^\circ\text{C}$, 2.5-38 h, 34-92 % yield ; f) TMS-alkyne, $\text{Pd}(\text{dppf})\text{Cl}_2 \cdot \text{CH}_2\text{Cl}_2$, CuCl, TMEDA:DMF=1:1, 80°C , 14.5-22 h, 53-78 % yield; g) K_2CO_3 , MeOH, rt, 2.5 h, 94 % yield.

Table 1. Biochemical and cellular characterization of FKBP12-FRB Molecular Glues. Affinities for compounds binding to purified human FKBP12 were determined by a competitive FP assay (K_i^{FP}).⁴⁹ Biochemical potencies for ternary complex induction were determined using a FP assay by titrating purified FRB with compound-bound fluorescently labelled FKBP12 ($\text{EC}_{50}^{\text{ternary FP}}$). Intracellular potencies for FKBP12 occupancy were determined by a competitive NanoBRET assay ($\text{IC}_{50}^{\text{NanoBRET}}$)⁵⁰ and potencies for intracellular formation of FKBP12-compound-FRB ternary complexes were determined by HEK293T cells transiently expressing a FKBP12-nLuc and FRB-HaloTag BRET pair ($\text{EC}_{50}^{\text{ternary nanoBRET}}$).

n.b. = non-binding, n.m. = not measured.

No.	human FKBP12 K_i^{FP} / nM ⁴⁹	$\text{EC}_{50}^{\text{ternary FP}}$ / μM	FKBP12 $\text{IC}_{50}^{\text{NanoBRET}}$ / nM ⁵⁰	$\text{EC}_{50}^{\text{ternary NanoBRET}}$ / nM ⁵¹	
rapamycin 1	0.6	0.039 ± 0.006	30.3 ± 1.5	1.8 ± 0.16	-
7	6.3	93 ± 21	81.2 ± 16.3	n.b.	

9a	5.8	56 ± 10	40.6 ± 5.3	n.m.	
9b	3.6	54 ± 6	47.8 ± 10.7	n.m.	
10a	11	50 ± 5	405 ± 219	n.b.	
10b	13	63 ± 6	101 ± 19	n.m.	
10c	5.1	7.8 ± 2.6	146 ± 28.5	n.b.	
10d	4.5	4.1 ± 0.4	25.5 ± 3.0	50.5 ± 9.8	
10e	6.9	2.0 ± 0.2	57.3 ± 16.8	38.8 ± 1.7	
10f	1.8	1.9 ± 0.2	259 ± 37	28.2 ± 1.3	
10g	4.7 ± 1.8	1.8 ± 0.1	49.2 ± 4.0	26.0 ± 1.6	
10h	0.8	1.5 ± 0.2	66.9 ± 22.5	31.7 ± 2.5	
10i	0.4	1.3 ± 0.2	264 ± 36.8	172 ± 36	
10j	7.2 ± 1.7	0.63 ± 0.06	799 ± 183	57.5 ± 3.6	
10k	4.1 ± 0.6	0.56 ± 0.03	314 ± 21	26.3 ± 1.3	
10l	4.5	0.53 ± 0.07	527 ± 77	32.9 ± 2.5	
10m	6.0	0.23 ± 0.03	952 ± 147	31.7 ± 2.1	
10n	4.8 ± 0.8	0.18 ± 0.02	1330 ± 195	42.1 ± 2.8	
10o	2.6	0.17 ± 0.02	7460 ± 2100	109 ± 6.3	

To test if the synthetic FKBP12-FRB molecular glues were active in cells, we performed a NanoBRET assay using nanoLuc-tagged FKBP12 and HaloTag-tagged FRB (Fig. 4A and Tab. 1). Compounds **10d-o** all dose-dependently induced the FKBP12-FRB complex in HEK293T cells, although more weakly than rapamycin **1**. This was FKBP12 binding-dependent since pretreatment with a high-affinity FKBP12 ligand abolished the NanoBRET signal (Fig. 4B). For all active analogs, the induction of the ternary complex in cells consistently occurred at similar concentrations (25-170nM), which were substantially lower than the ternary complex formation potencies determined biochemically. We attribute this to a combination of intracellular FKBP12 occupancy (reflected by the competitive NanoBRET assay) and the potency of the FKBP12-compound pre-complex to bind to FRB (reflected by the biochemically determined ternary complex formation, $EC_{50}^{\text{ternary FP}}$). The higher apparent potency for intracellular ternary complex formation can be explained by an excess of FKBP12-nLuc over FRB-Halo. Thereby, only a small fraction of FKBP12 occupancy is sufficient to produce a maximal NanoBRET signal. Interestingly, we observed a clear threshold for intracellular ternary complex formation, which was determined by biochemical ternary complex formation potency. Compounds with an $EC_{50}^{\text{ternary FP}} > 4.1 \mu\text{M}$ did not induced ternary intracellular NanoBRET signals while all compounds with an $EC_{50}^{\text{ternary FP}} < 4.1 \mu\text{M}$ did.

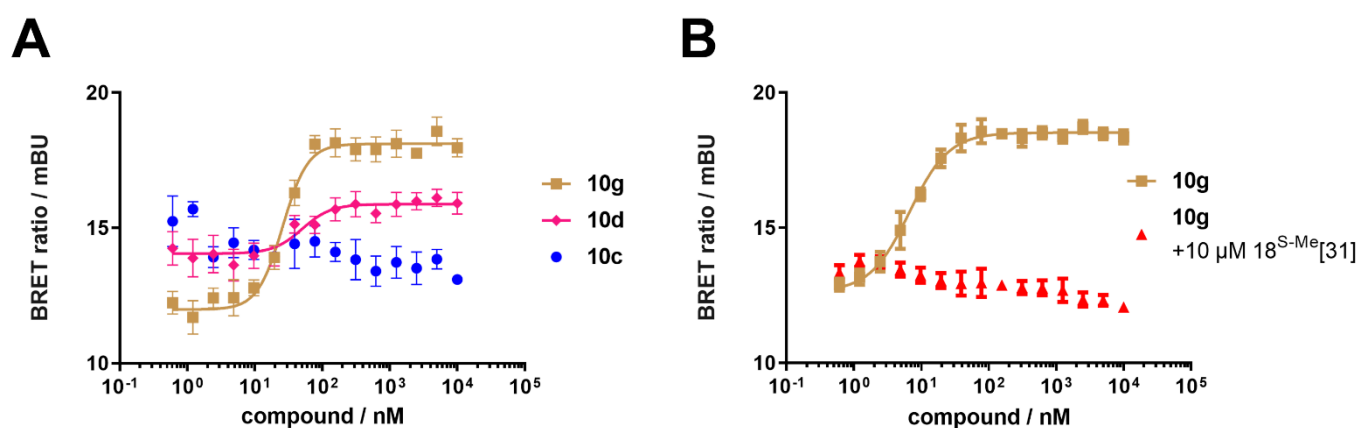


Figure 4. Cellular characterization of FKBP12-FRB molecular glues. **A** Compounds **10d** and **10g**-induced FKBP12-FRB ternary complex formation in HEK293T cells determined by NanoBRET assay using C-terminal NanoLuc-tagged FKBP12 and C-terminal HaloTag-tagged FRB, while compound **10c** did not. **B** Compound **10g**-induced FKBP12-FRB ternary complex formation in HEK293T cells is abolished by pre-treatment with a potent FKBP12 inhibitor (18^S-Me from Kolos et al.^[31]).

In conclusion, our screening approach enabled us to identify a novel molecular glue targeting the flat surface of the FRB-domain of mTOR. Screening at high target protein concentrations was crucial to identify an initially very weak hit, which would have been difficult to detect by other approaches. Although our approach was unbiased regarding the binding site on FRB, the identified molecular glues target a similar region on FRB as rapamycin **1**. The surface on FRB around Tyr²⁰²⁸/Phe²⁰³⁹, Val²⁰⁹⁴-Thr²⁰⁹⁸, and Trp²¹⁰¹-Phe²¹⁰⁵, while not *a priori* apparent, thus appeared to represent a preferred region for protein-protein contacts. Indeed, this site has been suggested to assist in the binding of mTOR targets such as S6K and PRAS40, as well as phosphatidic acid (PA)⁵². The preference for this region was not due to specific contacts with FKBP12, since in the context with compound **7**, FKBP12 engaged FRB in a completely different manner than in context with rapamycin **1**. However, as for rapamycin **1**, direct FKBP12-FRB contacts were crucial to dramatically enhance the affinity of the FKBP12-compound **7** complex to FRB compared to FRB-binding of the compound alone^{53,54}. The substantially higher affinity of the FKBP12-rapamycin **1** complex over the FKBP12-compound **7** complex for FRB is likely due to energetically more favorable interactions, where the rapamycin-FRB interactions appear to be more extensive and elaborate compared to the compound **7**-FRB contacts. Aided by the crystal structure we were able to improve the affinity of our initial hit by rational design up to 500-fold, leading to compounds which bind the FRB domain of mTOR at nanomolar concentrations in cells.

Our findings have several implications for the discovery of molecular glues: (i) Molecular glues might be less rare than initially thought as we found one hit within a relatively small, focused library. (ii) Screening approaches with high compound and presenter protein concentrations were necessary to find such weak molecular glue hits. Biochemical approaches seemed to be most adequate as weak activity is easier to detect compared e.g. to cellular assays. (iii) The use of a focused library targeted to the presenter protein (FKBP12 in our case) likely facilitated the identification of molecular glues substantially since part of the recognition problem was already pre-engineered. (iv) Weak initial molecular glue hits can be used as a starting point for rational design to get more potent molecular glues. Even for weak molecular glue hits, the ternary complex structure can be obtained, which facilitates optimization substantially. (v) Shallow hydrophobic surfaces seem to be a preferred interaction site for molecular glues, in line with the binding modes of rapamycin **1**, FK506 **2** and WBD002 **4**^{11-13,55}. (vi) At large excess of the presenter protein over the target protein, only a small fractional occupancy of the presenter protein might be sufficient to evoke the effect. (vii) The expression levels of the presenter protein represent a threshold

beyond which weak molecular glues cannot work in cells. (viii) The choice of the presenter protein is likely a key factor. FKBP12 (like Cyp18) might be a privileged presenter protein featuring high abundance in many tissues⁵⁶, absence of negative effects by binding of FKBP12 alone, availability of potent ligands as docking scaffolds, and numerous exit vectors on the latter. These features likely contributed to the prevalence of FKBP (and cyclophilins) as presenter proteins in nature and support their use to target otherwise undruggable proteins in drug discovery.

Methods:

Compound synthesis and characterization

If not indicated otherwise, reagents and solvents were purchased from commercial suppliers and used without further treatment. All reactions were followed by TLC analysis or LCMS. Flash silica gel column chromatography was performed with a Biotage® Isolera One system with Biotage® Sfär Silica HC Duo columns. Column chromatography was performed manually with silica gel 60 (0.04-0.063 mm) from Macherey Nagel GmbH & Co. KG. Semi-Preparative HPLC was performed with an Interchim PuriFlash 5250 system with a Luna® 5 µm C18(2) 100 Å, 250x21.2 mm column from Phenomenex. Eluents were 0.1 % TFA in water (Eluent A) and 0.1 % TFA in acetonitrile (Eluent B), methods are given in percentage of B. All key compounds were of >95 % purity by HPLC. Compound purity and low-resolution mass spectra were determined using an Agilent 1260 Infinity II system with a Poroshell 120 EC-C18 1.9 µm, 2.1 x 50 mm column from Agilent. Eluents were 0.1 % formic acid in water (Eluent A) and 0.1 % formic acid in acetonitrile (Eluent B), the used method was 5 % B to 100 % B in 2 min or 50 % B to 100 % B in 2 min or 70 % B to 100 % B in 2 min. MS was recorded with an Agilent InfinityLab G6125B LC/MSD. NMR spectroscopy was performed by the NMR department at TU Darmstadt. NMR spectra were recorded either on a 300 MHz Avance II NMR spectrometer from Bruker BioSpin GmbH (for ¹H-NMR only), a 300 MHz Avance III NMR spectrometer from Bruker BioSpin GmbH (for ¹H-, ¹³C-NMR), or a 500 MHz NMR spectrometer DRX 500 from Bruker BioSpin GmbH (for ¹H- and ¹³C-NMR). NMR spectra were recorded at room temperature. Chemical shifts are given in parts per million, referenced to the respective solvent (¹H: CDCl₃ = 7.26 ppm, [D₄]MeOH = 4.87 ppm, ¹³C: CDCl₃ = 77.16 ppm, [D₄]MeOH = 49.00 ppm). Coupling constants (*J*) are given in hertz (Hz), peak multiplicities are given as singlet (s), doublet (d), triplet (t), quartet (q) or multiplet (m). HRMS was performed by the mass spectrometry department at TU Darmstadt. Mass spectra were recorded on an Impact II, quadrupol-time-of-flight spectrometer from Bruker Daltonics. TLC was performed on TLC Silica gel 60 F254 Aluminum sheets from Merck Millipore. All final test compounds had a purity ≥95 % as determined by HPLC and UV detection at 220 nm.

Fluorescence resonance energy transfer (FRET) for the medium throughput screening and validation.

For most pipetting steps, a Beckman Coulter FXP Laboratory Automation Workstation was used. The compounds were used at a concentration of 100 µM with 1 % DMSO, the protein His-eGFP-FKBP12 was used at 100 µM, the FRB with GST-Tag was used at a concentration of 20 nM and the anti-GST-terbium-antibody was used at concentration of 1 nM. For each compound the percentage of possible ternary complex formation was measured two times. The percentage of possible ternary complex formation was determined by normalizing the fluorescence intensity of the His-eGFP-FKBP12 (535 nm) with anti-GST-terbium-antibody (620 nm). Each compound that exhibited a FRET-Signal of ≥0.15 was considered as hit and was further validated in a dose response experiment.

For the dose-response measurements, the compounds (200 µM in buffer (20 mM HEPES, pH 8.0, 0.002 % v/v Triton X-100, 150 mM NaCl) with 4 % DMSO) were diluted in a 1:2 serial dilutions and then mixed in triplicates with GST-FRB (20 nM), His-eGFP-FKBP12 (100 µM) and anti-GST-terbium-antibody (1 nM) in buffer (20 mM HEPES, pH 8.0, 0.002 % v/v Triton X-100, 150 mM NaCl) in a black,

non-binding 384-well plate, and then incubated for 30 min. Emission wavelengths of 535 nm and 620 nm were measured on a Tecan Spark at room temperature with an excitation wavelength of 340 nm.

Fluorescence polarization assays for the validation of the ternary complex

His-FRB and FKBP12^{E140C} were recombinantly expressed in *E.coli* BL21DE3Gold with a purity of >90 % as visually judged by Coomassie gel and SEC. The proteins were stored in buffer (20 mM HEPES, pH 8.0, 150 mM NaCl). FKBP12^{E140C} was labelled with fluorescein-5-maleimide. Excess dye was removed by PD10 columns and dialysis against 20 mM HEPES, pH 8.0, 150 mM NaCl.

The His-FRB were serial 1:2 diluted in assay buffer (20 mM HEPES, pH 8.0, 150 mM NaCl, 0.002 % Triton X-100) in a black, non-binding 384 well plate with a start concentration of 100 μ M and then mixed with 20 nM fluorescein-labelled FKBP12^{E140C} and 5 μ M ligand. Polarization was measured after incubation time for 30 min at room temperature with an excitation wavelength of 485 nm and an emission wavelength of 535 nm. The EC₅₀-values were determined by a four-parameter fitting by GraphPad Prism version 8.0 for Windows (GraphPad Software, La Jolla, CA).

In vitro photo crosslinking assay

FKBP12 constructs were recombinantly expressed in and purified from *E.coli* BL21DE3Gold. The mono cysteine mutations were labelled with maleimide-PEG-diazirine and desalted by PD10 columns. His-TEV-monoCys-FKBP12^{T43C}-diazirine-maleimide was mixed with GST-FRB in HEPES pH 8; 150 mM NaCl + 0.01 % Triton X so the end concentration of the FKBP12 construct was 50 μ M and the end concentration of GST-FRB was 250 nM. Compounds were added in desired concentrations and incubated on ice for 30 min. The samples were distributed in the wells of a 96 well polystyrene plate and irradiated on ice for 30 min by UV light (100-Watt, 365 nm). Samples were denatured by boiling in 4x Lämmli buffer and analyzed by Western Blot.

Native MS

Stock solutions of FKBP12 and FRB, as well as of each compound (rapamycin, compound **7** and compound **10k**), were prepared separately at a concentration of 50 μ M in deionized water. In native MS, a desalting step is typically required as proteins often form non-specific adducts with non-volatile salts and other interfering compounds. This causes MS peak broadening, which decreases resolution and jeopardizes accuracy, potentially preventing the correct peak assignment. ZebaTM spin columns with a molecular weight cut-off of 7 kDa were used to buffer-exchange the proteins to 200 mM aqueous ammonium acetate.

Working solutions of both proteins mixed with MG were prepared at 17 μ M in 200 mM ammonium acetate just before the MS analysis. The samples were sprayed with in-house-pulled glass needles via a static nano-electrospray ionisation source (nanoESI) coupled to a Waters Synapt XS mass spectrometer from Waters (USA). The glass needles were prepared using a P97 needle puller from Sutter Instrument Company (USA). For all samples, a capillary voltage in the range of 1.5–1.8 kV was used, while the source and desolvation temperatures were set at 30 °C and 200 °C, respectively. Two MS experiments were carried out: (i) MS1, where there is no isolation of a specific target in the instrument quadrupole, meaning that all ions can be seen in the spectrum; and (ii) MS2 (MS/MS), where a native charge state of the ternary complex was first isolated in the quadrupole region, and further activated by collision-induced dissociation (CID) to induce molecular dissociation of the respective subunits. This experiment is sometimes referred to as 'complex-up MS'. MS main parameters for Fig 2F: capillary voltage, 1.5 kV; source temperate, 30 °C; desolvation temperature, 200 °C trap collision

energy, 5 V; and transfer collision energy, 2 V. A more detailed description of the parameters used in the experiments of Fig. S5 can be found in the figure caption. The data were acquired and processed using the Masslynx 4.2 software package from Waters.

NanoBRET assay for determination of intracellular binding affinity to FKBP12⁵⁰

A FKBP ligand dilution series was performed at a 100-fold concentration of the final sample in DMSO. Next, the ligands were diluted to a 2-fold concentration required for the final sample in Opti-MEM reduced serum medium (gibco, REF 11058-021) and 20 μ l were transferred to a white non-binding 384 assay plate (greiner REF 781904). HEK293T cells stably expressing FKBP12-NanoLuc⁵⁰ were detached from a cell culture dish and suspended in Opti-MEM reduced serum medium at a concentration of 9.05×10^5 cells/ml. The fluorescent tracer [**2b** from Gnatzy et al.⁵⁰] was diluted to 160 nM and in Opti-MEM. Afterwards, a cell-tracer mixture was prepared by mixing 3 parts detached cells with one part of the 8-fold tracer dilution (e.g. 6.6 mL detached cells + 2.2 mL 8-fold tracer solution), yielding a 2-fold cell-tracer mix. 20 μ L of the 2-fold cell tracer mix were added on top of the compound solution to the assay plate, which is briefly spun down, sealed with aluminum foil and incubated at 37 °C for 2 h. Afterwards the assay plates were equilibrated at room temperature for 15 min. For BRET detection, 20 μ L of 7.5 μ M extracellular Nluc-Inhibitor (compound **43**⁵⁷) + 6.6 μ M furimazine (compound **26dl**⁵⁸) dissolved in Opti-MEM were added. The donor and acceptor emissions were measured at 445-470 nm and 610-700 nm in a well-wise measuring mode (Tecan Spark) for 1 sec, respectively. The IC₅₀-values were determined by a four-parameter fitting by GraphPad Prism version 8.0 for Windows (GraphPad Software, La Jolla, CA).

NanoBRET assay for ternary complex formation⁵¹

On the first day HEK293 cells were seeded 100000 cells ml⁻¹ with 3 ml per well into a 6-well plate coated with Poly-D-Lysine. On the second day the cells were transfected. 150 μ l OMEM containing 2.4 μ g acceptor plasmid and 600 ng donor plasmid per well were mixed with 150 μ l OMEM containing 22.5 μ g Polyethyleneimine per ml. The transfection mix was incubated for 25 min at room temperature. The medium on the plate was changed to 90 % of fresh DMEM medium and the transfection mix was added. Subsequently, cells were grown for 48 h. On the fourth day four the cell medium was exchanged for fresh DMEM Medium supplemented with 100 nM HALO Tag ligand and the cells were incubated overnight. On the fifth day the cells were washed with PBS and trypsinated for 2 min at 37 °C. The trypsin was quenched by addition of DMEM medium. The cells were precipitated by centrifugation and resuspended in OMEM to yield a suspension of 500000 cells ml⁻¹. Compounds were prepared in a dilution series in DMSO and mixed 1:100 with OMEM. 20 μ l dilution series of compounds was distributed on 384 well assay plates and 20 μ l cell suspension was added to the compounds. Afterwards the assay plates were equilibrated at room temperature for 15 min. For BRET detection, 20 μ L of 7.5 μ M extracellular Nluc-Inhibitor (compound **43**⁵¹) + 6.6 μ M furimazine (compound **26dl**⁵⁸) dissolved in Opti-MEM were added. The donor and acceptor emissions were measured at 445-470 nm and 610-700 nm in a well-wise measuring mode (Tecan Spark) for 1 sec, respectively. The EC₅₀-values were determined by a four-parameter fitting by GraphPad Prism version 8.0 for Windows (GraphPad Software, La Jolla, CA).

References

1. Schreiber, S. L. The Rise of Molecular Glues. *Cell* **184**, 3–9 (2021).
2. Schreiber, S. L. Molecular glues and bifunctional compounds: Therapeutic modalities based on induced proximity. *Cell Chem Biol* (2024).
3. Rui, H., Ashton, K. S., Min, J., Wang, C. & Potts, P. R. Protein-protein interfaces in molecular glue-induced ternary complexes: classification, characterization, and prediction. *RSC Chem Biol* **4**, 192–215 (2023).
4. Geiger, T. M., Schäfer, S. C., Dreizler, J. K., Walz, M. & Hausch, F. Clues to molecular glues. *Current Research in Chemical Biology* **2**, 100018 (2022).
5. Kozicka, Z. & Thomä, N. H. Haven't got a glue: Protein surface variation for the design of molecular glue degraders. *Cell Chem Biol* **28**, 1032–1047 (2021).
6. Sasso, J. M., Tenchov, R., Wang, D., Johnson, L. S., Wang, X. & Zhou, Q. A. Molecular Glues: The Adhesive Connecting Targeted Protein Degradation to the Clinic. *Biochemistry* **62**, 601–623 (2023).
7. Liu, S. et al. Rational Screening for Cooperativity in Small-Molecule Inducers of Protein-Protein Associations. *J Am Chem Soc* **145**, 23281–23291 (2023).
8. Mahalati, K. & Kahan, B. D. Clinical pharmacokinetics of sirolimus. *Clin Pharmacokinet* **40**, 573–585 (2001).
9. Suthanthiran, M., Morris, R. E. & Strom, T. B. Immunosuppressants: cellular and molecular mechanisms of action. *Am J Kidney Dis* **28**, 159–172 (1996).
10. Schreiber, S. L. Chemistry and biology of the immunophilins and their immunosuppressive ligands. *Science* **251**, 283–287 (1991).
11. Liu, J., Farmer, J. D., Lane, W. S., Friedman, J., Weissman, I. & Schreiber, S. L. Calcineurin is a common target of cyclophilin-cyclosporin A and FKBP-FK506 complexes. *Cell* **66**, 807–815 (1991).
12. Gaali, S., Gopalakrishnan, R., Wang, Y., Kozany, C. & Hausch, F. The chemical biology of immunophilin ligands. *Curr Med Chem* **18**, 5355–5379 (2011).
13. Schreiber, S. L. Immunophilin-sensitive protein phosphatase action in cell signaling pathways. *Cell* **70**, 365–368 (1992).
14. Brown, E. J. et al. A mammalian protein targeted by G1-arresting rapamycin-receptor complex. *Nature* **369**, 756–758 (1994).
15. Shigdel, U. K. et al. Genomic discovery of an evolutionarily programmed modality for small-molecule targeting of an intractable protein surface. *Proc Natl Acad Sci U S A* **117**, 17195–17203 (2020).
16. Chang, C.-F., Flaxman, H. A. & Woo, C. M. Enantioselective Synthesis and Biological Evaluation of Sanglifehrin A and B and Analogs. *Angew Chem Int Ed Engl* **60**, 17045–17052 (2021).
17. Pua, K. H., Stiles, D. T., Sowa, M. E. & Verdine, G. L. IMPDH2 Is an Intracellular Target of the Cyclophilin A and Sanglifehrin A Complex. *Cell Rep* **18**, 432–442 (2017).
18. Fehr, T. et al. Antascomicins A, B, C, D and E. Novel FKBP12 binding compounds from a *Micromonospora* strain. *J Antibiot (Tokyo)* **49**, 230–233 (1996).
19. Schäfer, S. C., Voll, A. M., Bracher, A., Ley, S. V. & Hausch, F. Antascomycin B stabilizes FKBP51-Akt1 complexes as a molecular glue. *Bioorg Med Chem Lett* **104**, 129728 (2024).
20. Salituro, G. M. et al. Meridamycin: A novel nonimmunosuppressive FKBP12 ligand from *Streptomyces hygroscopicus*. *Tetrahedron Letters* **36**, 997–1000 (1995).
21. Summers, M. Y., Leighton, M., Liu, D., Pong, K. & Graziani, E. I. 3-normeridamycin: a potent non-immunosuppressive immunophilin ligand is neuroprotective in dopaminergic neurons. *J Antibiot (Tokyo)* **59**, 184–189 (2006).
22. Guo, Z. et al. Rapamycin-inspired macrocycles with new target specificity. *Nat Chem* **11**, 254–263 (2019).
23. Guo, Z. et al. Discovery of a Potent GLUT Inhibitor from a Library of Rapafucins by Using 3D Microarrays. *Angew Chem Int Ed Engl* **58**, 17158–17162 (2019).
24. Park, H. et al. PAAN/MIF nuclease inhibition prevents neurodegeneration in Parkinson's disease. *Cell* **185**, 1943–1959 (2022).
25. Schulze, C. J. et al. Chemical remodeling of a cellular chaperone to target the active state of mutant KRAS. *Science* **381**, 794–799 (2023).

26. Jänne, P. A. et al. Abstract PR014: Preliminary safety and anti-tumor activity of RMC-6291, a first-in-class, tri-complex KRASG12C(ON) inhibitor, in patients with or without prior KRASG12C(OFF) inhibitor treatment. *Molecular Cancer Therapeutics* **22**, PR014-PR014 (2023).
27. Holderfield, M. et al. Concurrent inhibition of oncogenic and wild-type RAS-GTP for cancer therapy. *Nature* **629**, 919–926 (2024).
28. Wasko, U. N. et al. Tumour-selective activity of RAS-GTP inhibition in pancreatic cancer. *Nature* **629**, 927–936 (2024).
29. Jiang, J. et al. Translational and Therapeutic Evaluation of RAS-GTP Inhibition by RMC-6236 in RAS-Driven Cancers. *Cancer Discov* **14**, 994–1017 (2024).
30. Holdgate, G. A., Bardelle, C., Berry, S. K., Lanne, A. & Cuomo, M. E. Screening for molecular glues - Challenges and opportunities. *SLAS Discov* **29**, 100136 (2024).
31. Kolos, J. M. et al. Picomolar FKBP inhibitors enabled by a single water-displacing methyl group in bicyclic 4.3.1 aza-amides. *Chem Sci* **12**, 14758–14765 (2021).
32. Gopalakrishnan, R. et al. Exploration of pipercolate sulfonamides as binders of the FK506-binding proteins 51 and 52. *J Med Chem* **55**, 4123–4131 (2012).
33. Gopalakrishnan, R. et al. Evaluation of synthetic FK506 analogues as ligands for the FK506-binding proteins 51 and 52. *J Med Chem* **55**, 4114–4122 (2012).
34. Gaali, S. et al. Selective inhibitors of the FK506-binding protein 51 by induced fit. *Nat Chem Biol* **11**, 33–37 (2015).
35. Gaali, S., Feng, X., Hähle, A., Sippel, C., Bracher, A. & Hausch, F. Rapid, Structure-Based Exploration of Pipercolic Acid Amides as Novel Selective Antagonists of the FK506-Binding Protein 51. *J Med Chem* **59**, 2410–2422 (2016).
36. Feng, X. et al. A Novel Decalin-Based Bicyclic Scaffold for FKBP51-Selective Ligands. *J Med Chem* **63**, 231–240 (2020).
37. Feng, X., Sippel, C., Bracher, A. & Hausch, F. Structure-Affinity Relationship Analysis of Selective FKBP51 Ligands. *J Med Chem* **58**, 7796–7806 (2015).
38. Bischoff, M., Sippel, C., Bracher, A. & Hausch, F. Stereoselective construction of the 5-hydroxy diazabicyclo4.3.1decane-2-one scaffold, a privileged motif for FK506-binding proteins. *Org Lett* **16**, 5254–5257 (2014).
39. Bischoff, M., Mayer, P., Meyners, C. & Hausch, F. Enantioselective Synthesis of a Tricyclic, sp³-Rich Diazatetradecanedione: an Amino Acid-Based Natural Product-Like Scaffold. *Chemistry* **26**, 4677–4681 (2020).
40. Bauder, M. et al. Structure-Based Design of High-Affinity Macrocyclic FKBP51 Inhibitors. *J Med Chem* **64**, 3320–3349 (2021).
41. Pomplun, S. et al. Chemogenomic Profiling of Human and Microbial FK506-Binding Proteins. *J Med Chem* **61**, 3660–3673 (2018).
42. Pomplun, S., Wang, Y., Kirschner, A., Kozany, C., Bracher, A. & Hausch, F. Rational design and asymmetric synthesis of potent and neurotrophic ligands for FK506-binding proteins (FKBPs). *Angew Chem Int Ed Engl* **54**, 345–348 (2015).
43. Voll, A. M. et al. Macrocyclic FKBP51 Ligands Define a Transient Binding Mode with Enhanced Selectivity. *Angew Chem Int Ed Engl* **60**, 13257–13263 (2021).
44. Wang, Y. et al. Increasing the efficiency of ligands for FK506-binding protein 51 by conformational control. *J Med Chem* **56**, 3922–3935 (2013).
45. Kolos, J. Synthesis of tailor-made bicyclic [4.3.1] aza-amides. PhD thesis at <https://doi.org/10.26083/tuprints-00017571> (2023).
46. Purder, P. L. et al. Deconstructing Protein Binding of Sulfonamides and Sulfonamide Analogues. *JACS Au* **3**, 2478–2486 (2023).
47. Liang, J., Choi, J. & Clardy, J. Refined structure of the FKBP12-rapamycin-FRB ternary complex at 2.2 Å resolution. *Acta Crystallogr D Biol Crystallogr* **55**, 736–744 (1999).
48. Krissinel, E. & Henrick, K. Inference of macromolecular assemblies from crystalline state. *J Mol Biol* **372**, 774–797 (2007).
49. Kozany, C., März, A., Kress, C. & Hausch, F. Fluorescent probes to characterise FK506-binding proteins. *Chembiochem* **10**, 1402–1410 (2009).
50. Gnatzy, M. T. et al. Development of NanoBRET-Binding Assays for FKBP-Ligand Profiling in Living Cells. *Chembiochem* **22**, 2257–2261 (2021).
51. Machleidt, T. et al. NanoBRET--A Novel BRET Platform for the Analysis of Protein-Protein Interactions. *ACS Chem Biol* **10**, 1797–1804 (2015).
52. Yang, H. et al. Mechanisms of mTORC1 activation by RHEB and inhibition by PRAS40. *Nature* **552**, 368–373 (2017).
53. März, A. M., Fabian, A.-K., Kozany, C., Bracher, A. & Hausch, F. Large FK506-binding proteins shape the pharmacology of rapamycin. *Mol Cell Biol* **33**, 1357–1367 (2013).
54. Banaszynski, L. A., Liu, C. W. & Wandless, T. J. Characterization of the FKBP.rapamycin.FRB ternary complex. *J Am Chem Soc* **127**, 4715–4721 (2005).

55. Comment: The only reported rapamycin mimic with a non-FKBP-targeted scaffold is WRX606, identified by in silico screening (R. Shams, A. Matsukawa, Y. Ochi, Y. Ito, H. Miyatake, *J. med. chem.* 2022, 65, 1329). However, we did not observe FKBP12 binding or FKBP12-FRB dimerization in our biochemical assays for this compound (see supplement fig. S4).
56. Marinec, P. S., Chen, L., Barr, K. J., Mutz, M. W., Crabtree, G. R. & Gestwicki, J. E. FK506-binding protein (FKBP) partitions a modified HIV protease inhibitor into blood cells and prolongs its lifetime in vivo. *Proc Natl Acad Sci U S A* **106**, 1336–1341 (2009).
57. Walker, J. R. et al. Highly Potent Cell-Permeable and Impermeable NanoLuc Luciferase Inhibitors. *ACS Chem Biol* **12**, 1028–1037 (2017).
58. Coutant, E. P. et al. Bioluminescence Profiling of NanoKAZ/NanoLuc Luciferase Using a Chemical Library of Coelenterazine Analogues. *Chemistry* **26**, 948–958 (2020).
59. Cianci, M. et al. P13, the EMBL macromolecular crystallography beamline at the low-emittance PETRA III ring for high- and low-energy phasing with variable beam focusing. *J Synchrotron Radiat* **24**, 323–332 (2017).

Acknowledgements

We acknowledge funding by the iGLUE project of the PROXIDRUGS consortium (03ZU1109EB) and by the DFG (433472263 to FH, 524226614 to FL). The synchrotron data were collected at beamline operated by EMBL Hamburg at the PETRA III storage ring (DESY, Hamburg, Germany).⁵⁹ We would like to thank David von Stetten for the assistance in using the beamline. Edvaldo Maciel was supported by Humboldt fellowship. Synapt instrument was funded by DFG grant 461372424.

Author contributions

C.M. and F.H. developed the concept. R.C.E.D. and J.K. performed synthesis of the compounds. C.M. M.L.P., W.O.S., T.H., T.M.G. and S.K. contributed to biochemical assays. E.M. and F.L. carried out native mass spectrometry experiments. R.C.E.D. and F.H. wrote the manuscript with input from all authors.

Competing interests

The authors declare no competing interests.